Renewable Energy 136 (2019) 945–954

Contents lists available at ScienceDirect

Renewable Energy

journal homepage: www.elsevier.com/locate/renene

A model to include turbulence-turbulence interaction in the prediction of trailing edge far field noise for high angles of attack or slightly separated flow

Cordula Hornung*, Thorsten Lutz, Ewald Krämer

Institute for Aerodynamics and Gas Dynamics, Pfaffenwaldring 21, 70569 Stuttgart, Germany

ARTICLE INFO

Article history:
Received 29 November 2017
Received in revised form
12 December 2018
Accepted 26 December 2018
Available online 21 January 2019

Keywords:
Trailing edge noise
Turbulence-turbulence interaction
Separation
Noise prediction
High angles of attack

ABSTRACT

The most dominant noise source of modern wind turbines is considered to be trailing edge (TE) noise. TE noise increases with increasing angle of attack of the flow. For wind turbine development it is hence crucial to predict TE noise for high angles of attack up to slightly separated flow. It results from wall pressure fluctuations induced by turbulent vortices in the boundary layer. The source term for the pressure fluctuations consists of two terms, the interaction of the mean shear with the turbulence and the turbulence-turbulence interaction (TTI). TTI is neglected in the commonly used TE noise prediction model by Blake, resulting in a strong dependency of the model on the wall normal mean velocity gradient. With increasing angle of attack this wall normal gradient of the boundary layer diminishes. Hence the TTI of the source equation has to be taken into account in order to achieve reliable predictions towards higher angles of attack. Here a new simplified-analytical model including the TTI, based on the model deduction by Blake, is presented and compared to experimental data. It is found that the prediction quality for high angles of attack and slight TE separation can be improved with the new model.

1. Introduction

Wind turbine noise sources can be differentiated in mechanical and flow induced - i.e. aeroacoustic - noise. For modern wind turbines the main aeroacoustic sources are trailing edge (TE) and inflow turbulence noise, the latter being caused by the interaction of the leading edge with atmospheric turbulence. TE noise is often the dominant noise source of modern wind turbines. It is the result of turbulent vortices in the boundary layer which induce pressure fluctuations at the wall. They are convected in direction of the TE and there scattered to the surrounding far field (FF). In order to comply with the restrictive noise emission regulations, low noise airfoil and blade design is a crucial element in today's wind turbine blade development. It is thus very important to be able to predict the induced noise by the blades to gain insight into noise production already during the design process. Different methods can be distinguished to do so. They vary in computational effort and, reciprocally to that, in their flexibility to be applied to different aerodynamic situations. The most costly ones are computational aeroacoustics (CAA) methods, resolving the time as well as the space necessary for direct acoustic wave transmission. Since the involved frequencies are - compared to, for example, inflow noise - quite high and the length scales small applying CAA is extremely costly. It is therefore currently not a reasonable option during industrial design processes. Following the CAA in descending order of computational costs are the simplified analytical methods. Often based on standard RANS simulation they can be applied to a variety of different airfoil shapes and aerodynamic situations. They still represent the underlying physics quite well due to being derived from analytical equations. In general, the derivation is based on physical equations without any assumptions to the geometry other than the ratio between chord length and wave number. Thus, there are no limitations to the geometry as long as the flow physics stay the same. The geometric effects are included by means of the RANS simulation. For this reason the semi-analytical methods represent a good compromise between flexibility in application and computational costs. Next in row are the empirical methods. They are simple and especially fast and cheap to apply but they only deliver reliable results when being applied to flow situations which lie inside the range they were calibrated for. The last method, however slightly outside the afore mentioned categories, is the use of fully

* Corresponding author.
E-mail address: cordula.hornung@iag.uni-stuttgart.de (C. Hornung).

https://doi.org/10.1016/j.renene.2018.12.093
0960-1481/

Nomenclature

δ	boundary layer thickness
ε	dissipation
Λ_{22}	vertical integral length scale of wall normal fluctuations
ν	kinematic viscosity
ρ	density
τ_0	time scale from Pope for turbulent vortices
$\tau_{onsager}$	Onsager time scale for decay of turbulent vortices
Φ_{22}	normalized spectrum of wall normal velocity fluctuations
Φ_m	moving axis spectrum
ω	radial frequency
l_0	length scale
c_0	speed of sound
D	directivity
$f_{22,aniso}$	anisotropy factor
$E(k)$	Karman spectrum of energy
L	wetted length of airfoil
$k_0^2 = k_1^2 + k_2^2 + k_3^2$	total wave number
k_e	wavenumber of energy containing eddy
$\mathbf{k}, k_i$	wavenumber vector/wavenumber in x_i direction
k_T	turbulent kinetic energy
$P(k_1, k_3, \omega)$	power spectral density of wall pressure fluctuations
p'	pressure fluctuations
R	distance of observer
Re_λ	Re number of turbulent scales
$S(\omega)$	Sound pressure level
T_x	time scale of the moving axis spectrum
U_c	convection velocity
$\overline{U_i}$	mean velocity in x_i direction
u_i'	fluctuating velocity in x_i direction
u_p	"velocity" from the pressure gradient
x_i	coordinates (x_1 in mean flow, x_2 in wall normal direction)
$y+$	non-dimensionalized wall distance

analytical methods. They can be applied as long as it is possible to sufficiently simplify the problem statement.

Due to the advantages of semi-analytical methods, most methods presented in literature for the prediction of TE noise are based on models of this kind. The foundation for the semi-analytical TE models was laid by Blake and Parchen during the 80 ties and 90 ties of the last century. The aeroacoustic theory leading to the development of the models was described by Blake [1]. Parchen [2] was the first to propose a semi-analytical model for the prediction of airfoil TE noise, also known as the TNO model, afterwards. Two years later he put out an improved version [3]. Since then many papers concerning the enhancement of the original model were published (compare for example [4–7]). Anisotropy factors were introduced [6,8], different formulations for spectral parameters proposed [7] or alternative approaches suggested to determine the wall normal velocity fluctuations [9].

A disadvantage of these semi-analytical TNO models - all based on the same underlying equation - is that the prediction accuracy decreases when high angles of attack or high lift coefficients occur, associated with highly loaded boundary layers or the onset of separation. For the implementation developed by Kamruzzaman [8] for example it was shown in Ref. [10] that the dependency of the noise from the angle of attack is under-predicted. For a modern wind turbine high angles of attack occur in different flow situations, and might as well be desired by the turbine manufacturer to achieve high lift. Slightly separated flow can also occur e.g. within high atmospheric turbulence conditions or at high wind speed on the pressure side of the airfoil. It is, however, important to clearly distinguish those flow situations from stall - which is characterized by high flow separation with decrease of lift and vortex shedding -, which modern pitch controlled wind turbines are designed to avoid.

As a result, in literature some semi-empirical models accounting for the effects at high angles of attack and flow separation were proposed: In 2013 Schuele [11] published a semi-empirical extension for the Blake model. He uses a modified version of Coles law and the Prandtl mixing length approach to predict the modified vertical velocity fluctuations present in separated flow. Additionally, the spectra of the velocity fluctuations were fitted to measured data. Lastly the convection velocity was chosen in order to fit the measured FF data best with the predicted spectra. Bertagnolio [12] presented a semi-empirical approach for higher angles of attack. Measurements of pressure fluctuations were used to generate an empirical expression for the sound pressure of stall noise. It was found that for low Re the sound pressure scales with U_∞^3 whereas for higher Re this reduces to $U_\infty^{1/2}$. The model is dependent on the position of the separation point along the airfoil. Suryadi et al. [13] presented a heuristic approach to improve the prediction quality of the TNO model for Wall Pressure Fluctuation (WPF) spectra. They modified the model for the moving axis spectrum including two empirical constants which are dependent on the angle of attack. However, the three models can only be applied in presence of separation. Additionally they are empirical models with the disadvantages of such models sketched above.

The goal of the research presented here is to describe the theory and validation of a new model for TE noise prediction, providing a universal semi-analytical approach which can be applied to the entire angle of attack range of modern wind turbines with or without separation. It is thus also employable to the evaluation of 3D turbines in industrial design processes without previous knowledge of separation points. The application of the new model to a full scale wind turbine is presented in Ref. [14]. It is based on the method as proposed by Blake [1], with the underlying assumptions modified and the equations adapted accordingly. Note that stall noise with vortex shedding is out of the scope of the approach.

The results of the improved model will be compared to measurements conducted in different wind tunnels. FF noise measurements and predictions for different airfoils at various inflow velocities and angles of attack are evaluated. The new predictions are also compared to the results obtained with the former model by Kamruzzaman [8].

The paper is structured as follows. The general approach to determine noise spectra from CFD simulations is explained and the simulations and the experimental setups employed in the work are sketched in section 2. Subsequently, in section 3 the derivation of the new model equation is described and all model parameters are discussed. The resulting model is then applied to the example cases and compared to the measurements as well as to the predictions of the former model by M. Kamruzzaman. The results are shown in section 4. The paper ends with a discussion of the presented model and the conclusions.

2. Methods

The new model is developed in a similar manner as Blake [1] and Parchen's [3] TNO model. The model deduction is described in detail in the next section. TE noise of nine cases is predicted and compared to measurements in order to validate the model. Two different airfoils and Reynolds numbers ranging from 1.5 Mio. to 2.5 Mio. are evaluated. The main focus is on flow conditions with high angle of attack and slight TE separation.

2.1. Noise prediction

TE noise is predicted in this work using the in-house code IAGNoise+ of the Institute for Aerodynamics and Gas Dynamics (IAG) at the University of Stuttgart. IAGNoise + comprises three subprograms for TE noise prediction, the one used here for (quasi) 2D airfoils and two to predict the TE noise for three dimensional wind turbines. It is a completely revised, improved and newly programmed version of Rnoise, the code used by Kamruzzaman [7]. IAGNoise+ was further extended by the here presented new model equation and an alternative formulation of the anisotropy factor to be able to predict noise for high angles of attack and separated flow.

The prediction of TE noise in IAGNoise+comprises three steps (cf. Fig. 1). It is based on the evaluation of steady CFD RANS simulation results using the turbulent boundary layer characteristics. For this purpose a fully resolved boundary layer is necessary. The power spectrum of the WPF is modeled using the extracted parameters such as mean velocity or turbulent kinetic energy. Then the predicted WPF spectrum is integrated both along the streamwise and spanwise wavenumber direction as well as across the boundary layer to obtain a point frequency spectrum. This is then used as input to the FF model equation. The FF model applied in IAGNoise+ is the one developed by Chase [15] and Brooks & Hodgson [16]. It includes a directivity function to achieve the noise at any observer position desired.

The underlying source equation for the WPF is

$$\frac{\partial^2 p'}{\partial x_i^2} = -\rho \left(\underbrace{2\frac{\partial \bar{U}_i}{\partial x_j}\frac{\partial u_j'}{\partial x_i}}_{MTI} + \underbrace{\frac{\partial^2}{\partial x_i \partial x_j}\left(u_i' u_j' - \overline{u_i' u_j'}\right)}_{TTI} \right). \quad (1)$$

The first term on the right hand side describes the Mean-shear-Turbulence Interaction (MTI). The second term describes the influence of the Turbulence-Turbulence Interaction (TTI). As proposed by Blake, the TTI term is commonly neglected since the ratio of MTI to TTI is assumed to be at least 10 [1]. All models mentioned above are based on this assumption. The resulting models therefore mainly depend on the mean velocity gradient. With increasing angle of attack, however, the velocity gradient next to the wall at the TE decreases. This results in a diminishing source term and hence decreasing predicted wall pressure fluctuations. Therefore it seems reasonable to include the TTI term into the model for TE noise prediction, especially when looking at highly loaded boundary layers.

Panton and Linebarger [17] showed that in the low frequency range, below $k_1\delta = 0.5...1$ (with k_1: Streamwise wavenumber and δ: Boundary layer thickness) TTI is of the same order of magnitude as the MTI, although the predicted wavenumber range would be below the area of interest of most modern wind turbines. According to Kim [18], however, TTI is important also for non-separated boundary layers. He examined a channel flow at *Re* 3300. Pressure statistics revealed that across the entire tunnel width (for $y^+ > 15$) the nonlinear part - corresponding to TTI - of the pressure fluctuations is higher than the linear (MTI) contribution. When looking at specific source terms, Kim found that the TTI has higher influence on the pressure fluctuations than the MTI term and that the correlation between MTI and TTI is very small. It can be concluded that TTI has an influence on the WPF. Lee et al. [19] already included TTI in the model for WPF of reattached flow and could improve the prediction quality. However, they assumed the TTI to be dependent on the MTI and hence also on the velocity gradient normal to the wall. Due to that reason and the small correlation between MTI and TTI as noted in Ref. [18] a different approach is considered here. Both source terms are fully modeled independently of each other.

Higher angles of attack usually go hand in hand with higher pressure gradients strongly influencing turbulent anisotropy. For adverse pressure gradients the diffusion rate of the turbulent kinetic energy towards the wall increases, leading to lower anisotropy next to the wall [20]. Additionally turbulent structures are tilted to the wall normal direction increasing wall normal fluctuations throughout the boundary layer [20]. This leads to an increase of wall pressure fluctuations, the source of TE noise [21]. The spectral distribution, however, is not affected by this change in anisotropy [22]. Therefore the anisotropy formulation developed by Kamruzzaman [7] is extended to include pressure gradient effects. An anisotropy model including the local pressure gradient was also proposed by Ref. [6]. However, it was decided to rather extend the current model already included in the in-house code IAGNoise + instead of completely changing the anisotropy approach.

2.2. CFD simulation

All CFD simulations are conducted with FLOWer assuming steady flow. FLOWer is a RANS CFD code developed by the German Aerospace Center (DLR) for application to structured grid simulations of airfoils or turbines [23]. Since one of the goals of the proposed method is to apply it to the noise prediction of whole turbine rotors, it was decided to use RANS simulations as a flow simulation basis. Due to computational effort and costs for the time being aerodynamic and acoustic design of wind turbine blades have to rely on BL or RANS codes instead of high resolution methods. Furthermore, it was shown that the boundary layer characteristics necessary for noise prediction are predicted reliably by RANS methods with the necessary accuracy to measurements. Lutz et al. [10] for example show the comparison between measured and simulated boundary layer parameters close to the TE. To ensure the correct simulation of the underlying flow physics for the cases presented here, the boundary layer velocity profiles were

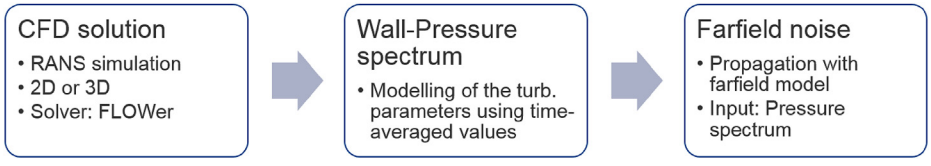

Fig. 1. Noise prediction with IAGNoise+.

compared to measurements as well. The two-equation Menter SST turbulence model is applied for the results presented here, although one equation models, e.g. SALSA, might be better in separation location prediction. However, two-equation models are more reliable in the prediction of turbulent parameters which are essential for TE noise prediction. The boundary layer is resolved with a $y^+_{wall} \approx 0.4$ and approximately 50 cells across the layer. Depending on *Re*, between 180 and 240 cells are used along the suction and pressure side of the airfoil, respectively. They are distributed with an increase in resolution at leading and trailing edge resulting in at least five cells between the evaluation point for the WPF and the TE.

For optimal accuracy of the noise prediction the evaluation point of the boundary layer should be located very close to the TE. Hence an evaluation point of 99.97 ± 0.01% of the chord length is selected.

2.3. Experiments

The experimental FF noise data used for validation are taken from two different measurement campaigns. The TL-231 measurements were conducted at the laminar wind tunnel (LWT) of the IAG using the coherent particle velocimetry (CPV) method [24]. The LWT is an open return wind tunnel with a closed test section with a very low turbulence intensity of less than $2 \cdot 10^{-4}$ [24]. In the CPV method special hot-wires are used to measure the particle velocity. Due to the characteristic phase difference of the cross-correlation function the noise emitted by the TE can then be separated from the background noise, under the assumption of a monopole type source [24]. A picture of the experimental setup is shown in Fig. 2.

The TL231 is an airfoil with 19% thickness which was developed for natural transition and high *Re* numbers. The measurement campaign was, however, conducted at comparably small *Re* and mostly tripped flow. This leads to cases with early separation. Slight TE separation is encountered at 98.7% of the airfoil (cf. Table 1) at an angle of attack of 0° already. Hence the cases used here represent highly loaded boundary layers, although it was only measured up to an angle of attack of 4.5°. In addition to the noise measurements hotwire measurements of the velocity distribution within the boundary layer were conducted.

For the NACA 0012 airfoil another campaign is used, carried out at the AWB wind tunnel in Braunschweig using array measurement. Those measurements were already presented in the benchmark study BANC II [5]. For a detailed description of the experiments and the corresponding setup the reader is referred to Ref. [25]. Experiments are assumed to have an uncertainty range of ±3 *dB* which was an outcome of the BANC II workshop [5] comparing measurements from different wind tunnels. The measured FF noise is in general specified for an observer 1 m above the airfoil with an angle of 90° to both trailing edge and chord line.

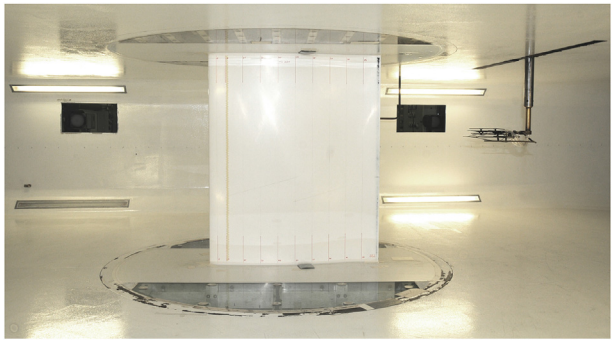

Fig. 2. Measurement setup (Picture from LWT Stuttgart, W. Wuerz).

Table 1
TL231 cases, measured in the LWT Stuttgart.

Test Case TL231_	*Re* $\cdot 10^6$	α [°]	x_{trans} [%] ss/ps	x_{sep} [%] sim. ss
45_00t	1.65	0	5/10	98.7
45_35t	1.65	3.5	5/10	98.2
45_45t	1.65	4.5	5/10	97.7
70_00t	2.55	0	5/10	99.1
70_35t	2.55	3.5	5/10	98.7
70_45t	2.55	4.5	5/10	98.4

Unfortunately for most experiments, the peak of the frequency spectra is not captured because of its location outside the measurement frequency range.

3. Modeling

As proposed in Refs. [15,16] the sound radiated at the TE of an airfoil can be calculated based on the WPF via

$$S(\omega) = \frac{L}{2\pi R^2} D \int_0^\infty \frac{\omega}{c_0 |k_1|} \frac{P(k_1, k_3 = 0, \omega)}{1 - \frac{\omega}{c_0 |k_1|}} dk_1. \tag{2}$$

Parchen [2] neglected the second term in the integrand's denominator, which is only valid for low Mach numbers. In this equation ω describes the frequency and k_1, k_3 the wavenumbers in the streamwise and spanwise direction, respectively. The sound velocity is depicted by c_0 and L is the wetted length in spanwise direction. The power spectrum of the WPF $P(k_1, k_3, \omega)$ needs to be modeled. The directivity D describes the dependency of the noise level at the observer position from the location of the noise source.

Roughly, an equation for the WPF is derived in four steps. First a differential equation is deduced from the Navier-Stokes-equations and the decomposition of velocity and pressure into their mean and fluctuating part is performed. This relation is then simplified and reduced. Afterwards, by the use of an ansatz function and a Fourier transformation in space and time, a solution of the reduced differential equation can be found. Finally, the remaining unknown terms e.g. the spectrum of the vertical velocity fluctuations, are modeled [1,2].

For the first step, with the assumption of incompressibility and constant viscosity in space, the equation describing the pressure gradient can be deduced with the divergences of the equation of momentum and the continuity equation resulting in

$$\frac{\partial^2 p}{\partial^2 x_i^2} = -\rho \frac{\partial^2 U_i U_j}{\partial x_i \partial x_j}. \tag{3}$$

By decomposing the pressure and the velocity into their mean and fluctuating parts, the source equation (eq. (1)) for pressure fluctuations is obtained. It is rewritten here for better readability.

$$\frac{\partial^2 p'}{\partial x_i^2} = -\rho \left(\underbrace{2 \frac{\partial \overline{U_i}}{\partial x_j} \frac{\partial u_j'}{\partial x_i}}_{MTI} + \underbrace{\frac{\partial^2}{\partial x_i \partial x_j} (u_i' u_j' - \overline{u_i' u_j'})}_{TTI} \right)$$

Splitting the TTI part and applying the continuity equation leads to

$$\frac{\partial^2}{\partial x_i \partial x_j} \left(u_i' u_i' - \overline{u_i' u_i'} \right) = \frac{\partial}{\partial x_i} u_i' \frac{\partial}{\partial x_j u_i'} - \frac{\partial^2}{\partial x_i \partial x_j} \left(\overline{u_i' u_i'} \right) \tag{4}$$

For the next steps a close look needs to be taken only at the time dependent first term in the equation. It can be written without Einstein's notation as

$$\frac{\partial^2}{\partial x_i \partial x_j}\left(u_i' u_j'\right) = \left(\frac{\partial}{\partial x_1}u_1'\right)^2 + \left(\frac{\partial}{\partial x_2}u_2'\right)^2 + \left(\frac{\partial}{\partial x_3}u_3'\right)^2 + 2\frac{\partial}{\partial x_1}u_2'\frac{\partial}{\partial x_2}u_1' + 2\frac{\partial}{\partial x_2}u_3'\frac{\partial}{\partial x_3}u_2' + 2\frac{\partial}{\partial x_1}u_3'\frac{\partial}{\partial x_3}u_1' \tag{5}$$

where x_1 is the streamwise, x_2 the wall normal and x_3 the spanwise direction, respectively. According to Ref. [18] the main source for WPF is $\frac{\partial}{\partial x_2}u_3'\frac{\partial}{\partial x_3}u_2'$. The spanwise wave number is set to zero for the determination of farfield noise (cf. eq. (2)). Derivatives in x_3 direction leading to k_3 components when being Fourier transformed can hence be neglected.

In order to identify the most relevant source terms in equation (5) a large eddy simulation (LES) of a NACA0012 with 40 m/s inflow velocity and $Re = 100\,000$ is examined. The simulation was conducted by D. Flad using the DGSEM FLEXI code [26]. The code uses a 12th order spectral element approach resulting in 32 Mio. Degrees of freedom with the 8550 hexahedral cells used. The average $y+$ after the trip on the suction side, based on the first integration point was 1.29, with the maximum being $y+ = 2.2$. Based on the equidistant inner cell distribution the average $y+$ was 4.9 (max. 8.3), the $x+ \approx 26$ and the average $z+ = 16.4$ (max 26.8). Note that the spacing in x-direction was not kept constant due to stretching. A sketch of the corresponding computational domain is shown in Fig. 3. The FF boundary is 75–100 chord lengths away. At the FF an acoustic damping zone was used to prevent any reflection of sound waves [27]. The simulation time was set to 38 times the convective time of the airfoil. The evaluation of the fluctuations is conducted over the rearmost ten percent of the suction side. The spatial derivatives are determined using a first order approach. 51 points are used in chord wise direction. In wall normal direction approximately 20 evaluation points are selected, all located inside the boundary layer.

The resulting source components for the FF are plotted in Fig. 4(a)–4(c) for the evaluated area. When comparing the figures with each other it becomes evident that the highest contribution is due to the cross-velocity term $2\frac{\partial u_2'}{\partial x_1}\frac{\partial u_1'}{\partial x_2}$. For this reason, the other terms are neglected in the following equations. Then, the model equation with the most relevant components for WPF and FF noise for the TTI reads:

$$\left[\frac{\partial^2 p'}{\partial x_i^2}\right]_{TT} = -\rho\left[2\frac{\partial}{\partial x_1}u_2'\frac{\partial}{\partial x_2}u_1' + 2\frac{\partial}{\partial x_2}u_3'\frac{\partial}{\partial x_3}u_2' - \frac{\partial^2}{\partial x_i \partial x_j}\left(\overline{u_i' u_j'}\right)\right] \tag{6}$$

The reduced differential source term equation can be solved by the use of the same ansatz function that Blake proposed [1] for the "only-MTI" equation:

$$p'(\mathbf{x},t) = -\frac{\rho}{2\pi}\cdot\int_V\left[\frac{\partial \overline{U_1}}{\partial x_2}\frac{\partial u_2'}{\partial x_1} + 2\frac{\partial}{\partial x_1}u_2'\frac{\partial}{\partial x_2}u_1' + 2\frac{\partial}{\partial x_2}u_3'\frac{\partial}{\partial x_3}u_2' - \frac{\partial^2}{\partial x_i \partial x_j}\left(\overline{u_i' u_j'}\right)\right]\frac{dV}{r} \tag{7}$$

In the next step the ansatz is transferred to the wavenumber frequency space in the x_1 and x_3 direction.

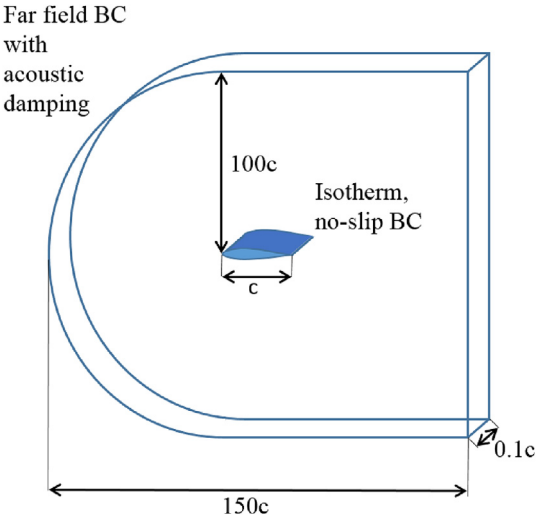

Fig. 3. Computational domain for the LES simulation.

$$\mathfrak{F}\{p'\} = -2\rho i\int_0^\infty \mathfrak{F}\{[\ldots]\}e^{ix_2\sqrt{k_0^2-k_1^2-k_3^2}}\frac{k_1}{\sqrt{k_0^2-k_1^2-k_3^2}}dx_2 \tag{8}$$

The Fourier transform of the inner part results in

$$\mathfrak{F}\{[\ldots] = \left[\mathfrak{F}\left\{u_2'\right\}\cdot\left(k_1\frac{\partial \overline{U_1}}{\partial x_2} + k_1\frac{\partial u_1'}{\partial x_2} + k_3\frac{\partial u_3'}{\partial x_2}\right)\right]. \tag{9}$$

Since the last term in eq. (7) is constant in time it becomes zero. The power density spectrum is the square of the pressure fluctuations spectrum. With the vertical velocity fluctuations modeled according to Blake [1], the equation results in

$$P(k_1,k_3,\omega) = 4\rho^2\left(\frac{1}{k_1^2+k_3^2}\right)\cdot\int_0^\infty\left(k_1^2\frac{\partial \overline{U_1^2}}{\partial x_2} + k_1^2\frac{\partial u_1'^2}{\partial x_2} + k_3^2\frac{\partial u_3'^2}{\partial x_2}\right)\tilde{\Phi}_{22}(k_1,k_3,\omega;x_2)\cdot e^{-2|\mathbf{k}x_2}dx_2. \tag{10}$$

The correlation between TTI and MTI is assumed to be negligible compared to the remaining terms. As stated above, the correlations between the TTI source terms are very small [18]. Hence the quadratic interaction terms are neglected for the FF noise prediction.

In the last step a model needs to be found for the resulting squared derivatives of the streamwise and spanwise velocity fluctuations. Under the assumption of homogeneous and isotropic dissipation, which is valid for small scale turbulence, it can be shown that [28].

$$\left(\frac{\partial u_1'}{\partial x_2}\right)^2 = \left(\frac{\partial u_3'}{\partial x_2}\right)^2 = 2\left(\frac{\partial u_1'}{\partial x_1}\right)^2. \tag{11}$$

With

$$\varepsilon = 15\nu\left(\frac{\partial u_1'}{\partial x_1}\right)^2 \tag{12}$$

this leads to

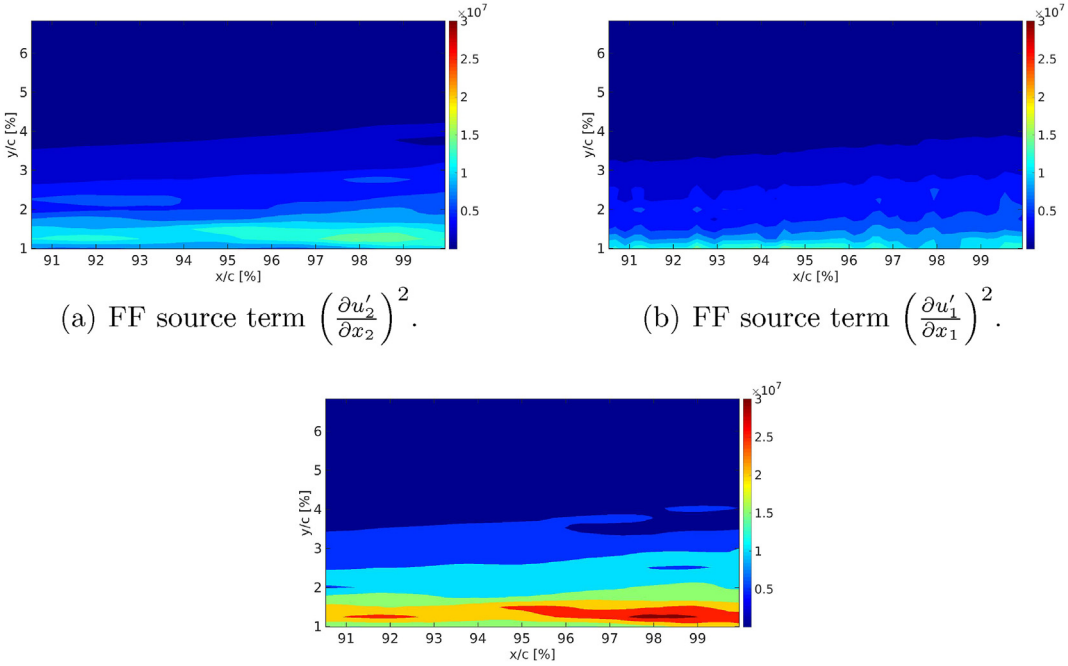

(a) FF source term $\left(\frac{\partial u_2'}{\partial x_2}\right)^2$.

(b) FF source term $\left(\frac{\partial u_1'}{\partial x_1}\right)^2$.

(c) FF source term $2\frac{\partial u_2'}{\partial x_1}\frac{\partial u_1'}{\partial x_2}$.

Fig. 4. TTI FF source terms for WPF equation.

$$\left(\frac{\partial u_1'}{\partial x_2}\right)^2 = \left(\frac{\partial u_3'}{\partial x_2}\right)^2 = \frac{2}{15\nu}\varepsilon. \tag{13}$$

The resulting model equation does now include the MTI as well as the TTI term. Both effects are present in every BL, only the ratio between the two contribution changes based on the BL characteristics. Thus the model equation (10) can be applied for low as well as for high angles of attack. The velocity gradient in the equation can be directly determined from the RANS simulation's velocity profile. However, the power spectral density of the vertical velocity fluctuations $\tilde{\Phi}_{22}$ has to be modeled. For this purpose the four dimensions are separated according to Blake [1]. The spectrum is then divided into the normalized three dimensional spectra of the velocity fluctuations $\Phi_{22}(k_1, k_3; x_2)$ and the moving axis spectrum $\Phi_m(\omega - k_1 U_c)$. The moving axis spectrum accounts for the distortion of the turbulent vortices when being convected in direction of the trailing edge. Further modeling parameters required are the Reynolds stresses $u_2^2(x_2)t$ of the vertical velocity fluctuations as well as the vertical integral length scale $\Lambda_2(x_2)$. As an alternative the variation as proposed by Fischer [9] without the separation approach can be used here. Filling the results back into equation (10), the final model equation for the power density of the WPF can be stated as:

$$P(k_1, k_3, \omega) = 4\rho^2\left(\frac{1}{k_1^2 + k_3^2}\right) \cdot \int_0^\infty (k_1^2(\frac{\partial \overline{U_1}}{\partial x_2}\right)^2 + \frac{2\left(k_1^2 + k_3^2\right)}{15\nu}\varepsilon)\Lambda_2\Phi_{22} \cdot \left\langle u_2'^2 \right\rangle \Phi_m e^{-2|\mathbf{k}x_2} dx_2 \tag{14}$$

The modeling parameters are chosen according to Ref. [8]:

$$\begin{aligned} \Phi_m &= \frac{T_x}{\sqrt{2\pi}} exp\left(-\frac{1}{2}(\omega - k_1 U_c)^2 T_x^2 \right) \\ \Phi_{22} &= \frac{4}{9\pi} \frac{k_e^{\frac{2}{3}}\left(k_1^2 + k_3^2\right)}{\left[k_e^2 + k_1^2 + k_3^2\right]^{\frac{7}{3}}} \\ \text{with} \quad k_e &= 0.748\Lambda_2 \\ \Lambda_2 &= \frac{1}{1.33368\varepsilon}\left[f_{22,aniso} \cdot \frac{2}{3}k_T\right]^{\frac{3}{2}} \\ U_c &= 0.7U_{loc} \end{aligned} \tag{15}$$

The convection velocity is negative in the lower part of the boundary layer for separated flow. Since the wavenumber spectrum is symmetric about the amplitude axis its absolute value can be used for the determination of the wavenumbers in dependency of the frequency. In all the other cases where the convection velocity is needed the negative values are used, as they represent the physical behavior. The anisotropy factor $f_{22,aniso}$ is modeled by

$$f_{22,aniso} = Re_\lambda^{-0.09} \cdot exp\left(\frac{u_p}{0.09U_e}\right) \tag{16}$$

where the first term is the anisotropy model as proposed by Kamruzzaman [8] and the second term is the newly introduced extension for the pressure gradient, with

$$Re_\lambda = \frac{\sigma\lambda_g}{\nu} \quad \text{and} \quad u_p = \left(\frac{\nu}{\rho}\frac{dp}{dx_1}\right)^{1/3} \tag{17}$$

using

$$\sigma = \sqrt{\frac{2}{3}k_T} \quad \text{and} \quad \lambda_g = \sqrt{\frac{10\nu k_T}{2\varepsilon}}. \tag{18}$$

Table 2
NACA 0012 cases, measured in the AWB.

Test Case NAC12_	Re $\cdot 10^6$	α [°]	x_{trans} [%] ss/ps	x_{sep} [%] sim. ss
60_00t	1.54	0	9.25	–
60_50t	1.54	5	6.96/9.25	99.9
60_76t	1.54	7.6	2.76/9.25	99.8

The timescale T_x is obtained using a combination of the memory time of turbulence as suggested by Ref. [7] and the Onsager scale representing the decay of turbulent vortices [29]:

$$T_x = \sqrt{\tau_0 \cdot \tau_{onsager}}$$
$$\tau_0 = \frac{l_0}{U} = \frac{2\Lambda_{22}}{U} \tag{19}$$
$$\tau_{onsager} = \frac{1}{\sqrt{k_1^3 E(k)}}$$

$E(k)$ is modeled herein according to Kolmogorov. All necessary parameters for the models can be extracted from RANS CFD simulations.

4. Results and discussion

The results, predicted with the new model equation, are compared to experimental data within this section. In the simulations as well as in the experiments the transition was enforced at a specific location along the first 10% of the chord. The reason for this was to gain a controlled state of the turbulent boundary layer at the TE. The exact tripping positions can be found in Tables 2 and 1. In order to ensure the same flow situation is achieved at the TE in the experiments and the FLOWer CFD simulations, the boundary layer's velocity profiles in streamwise direction are compared. For the cases with the TL-231 airfoil the profiles are shown in Fig. 5(a)–5(f). They were evaluated approximately 1 mm after the TE. The slight under prediction of the separation at the TE with the Menter SST model can be noted, which results in a steeper gradient of the boundary layer profile on the suction side. However, although the deviation increases slightly with higher angles of attack, the considered cases still show a reasonably good agreement between experiment and simulation to assume the same boundary layer state. Also for the NACA0012 the velocity profiles coincide. The corresponding comparisons were already published in e.g. Refs. [5,10]. Thus it is reasonable to use the results from the

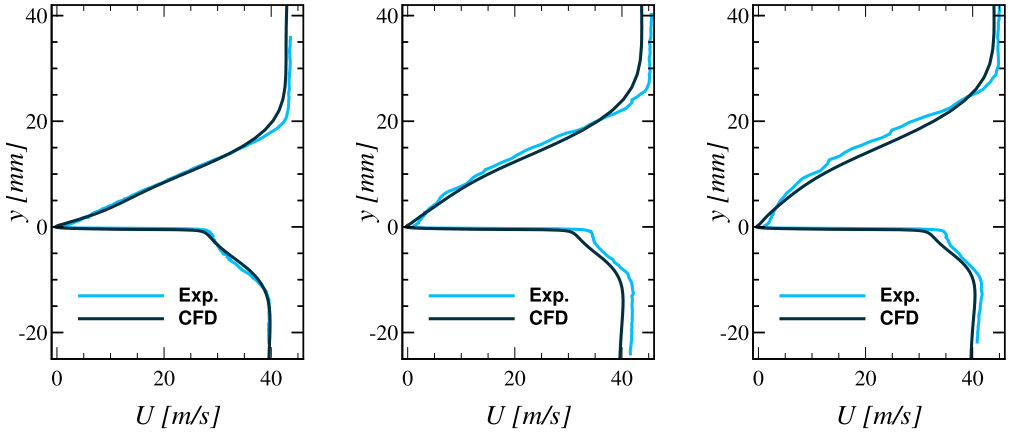

(a) Case TL231_45_00tSST with $U_\infty = 45\frac{m}{s}$ and $AoA = 0.0°$.

(b) Case TL231_45_35tSST with $U_\infty = 45\frac{m}{s}$ and $AoA = 3.5°$.

(c) Case TL231_45_45tSST with $U_\infty = 45\frac{m}{s}$ and $AoA = 4.5°$.

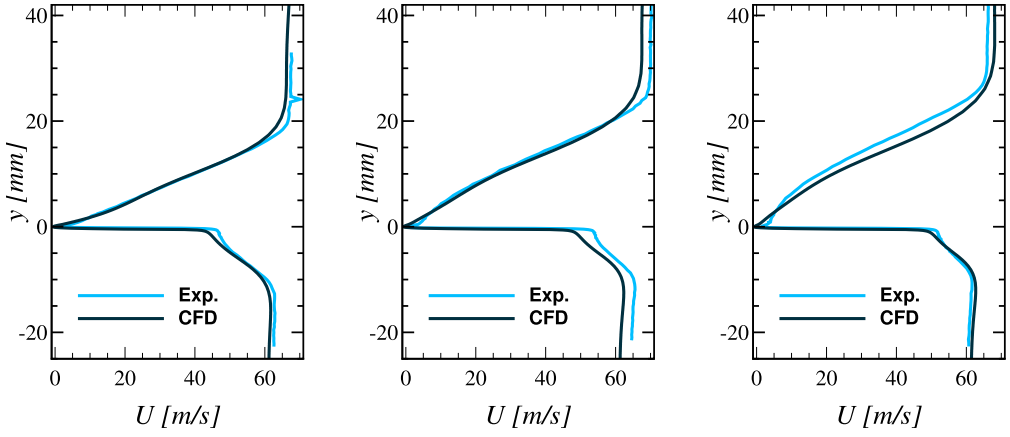

(d) Case TL231_70_00tSST with $U_\infty = 70\frac{m}{s}$ and $AoA = 0.0°$.

(e) Case TL231_70_35tSST with $U_\infty = 70\frac{m}{s}$ and $AoA = 3.5°$.

(f) Case TL231_70_45tSST with $U_\infty = 70\frac{m}{s}$ and $AoA = 4.5°$.

Fig. 5. Comparison of experimental and simulated (CFD) boundary layer profiles approx. 1 mm after the TE (Measurements from LWT Stuttgart, W. Wuerz).

simulations as input to the noise model.

Fig. 6(a)–6(c) show the TE noise spectra for three TL231 cases. The spectra predicted with the new model, the spectra resulting from the model proposed by Kamruzzaman (MK model) as well as the experimental results from CPV measurements with uncertainty bars are depicted. Due to confidentiality reasons the y-axis values are suppressed. As mentioned above, incipient TE separation can already be seen in the experiment and the simulation for the 0° angle of attack cases for this airfoil. Since the evaluation position for the TE noise is located very close to the TE at 99.5% chord, for all TL231 cases this point is located within the separated region of the simulations. Thus, the noise prediction includes the effects from the separated boundary layer. The exact separation positions are specified in the case table, Table 1. The transition positions of the simulations are chosen according to the tripping positions of the experiments.

While the results predicted by the MK model match the experimental data quite well for the 0° angle of attack case, a deviation for higher angles of attack (Fig. 6(b) and (c)) can be seen for the low frequencies. With the new model formulation the increase in noise with increasing boundary layer loadings on the suction side is captured quite well, as far as measured points are concerned.

The lower frequencies of the noise spectrum are generally considered to correspond to the noise produced on the suction side, whereas the higher frequency parts of the spectrum are related to the pressure side. Unfortunately it is quite difficult to measure TE noise correctly for lower frequencies. For the CPV method 1000 Hz is often the lower limit to gain valid data. For higher boundary layer loads or lower Reynolds numbers the peak frequency shifts towards lower ranges due to larger separation, leading to an inability to capture the noise peak. Instead, the pressure side noise production overweights the noise produced by the suction side.

Fig. 7(a)–7(c) show the same angles of attack, but at a lower Reynolds number, leading to larger separation. As for the 70 m/s cases, the suction side frequencies and the corresponding increase in noise with higher loadings are captured quite well. However, the experimental data is lacking information about the suction side apart from a few points indicating the ascent to the overall peak, which equals the suction side peak. The pressure side prediction quality decreases towards the higher angles of attack. This is especially visible in Fig. 7(c). The worse prediction quality of the pressure side is already a known disadvantage of the TNO model. It worsens with higher angles of attack and therefore stronger flow acceleration on the pressure side. However, the pressure side contribution rapidly becomes negligible when looking at the sound pressure levels.

In order to show the behavior of the modified approach for different airfoils and in comparison with measurements from a different wind tunnel, noise spectra measured in the AWB wind tunnel and the corresponding predictions for a NACA 0012 airfoil are depicted in Fig. 7(d)–7(f) [5]. Almost no separation is present (cf. Table 2) for the presented cases even though they cover a wider range of angles of attack than the TL231-cases. The new model is able to capture the increase in noise with angle of attack for these

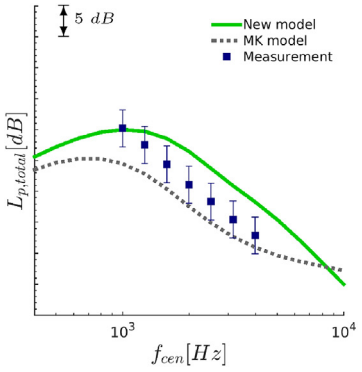

(a) Case TL231_70_00tSST corresponding to $U_\infty = 70\frac{m}{s}$ and $AoA = 0.0°$.

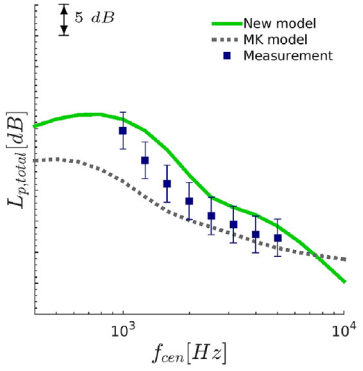

(b) Case TL231_70_35tSST corresponding to $U_\infty = 70\frac{m}{s}$ and $AoA = 3.5°$.

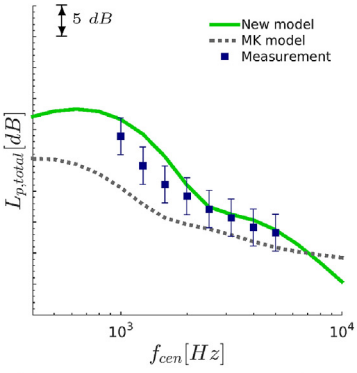

(c) Case TL231_70_45tSST corresponding to $U_\infty = 70\frac{m}{s}$ and $AoA = 4.5°$.

Fig. 6. Comparison of experimental and predicted (new model vs. model by M. Kamruzzaman) FF noise spectra.

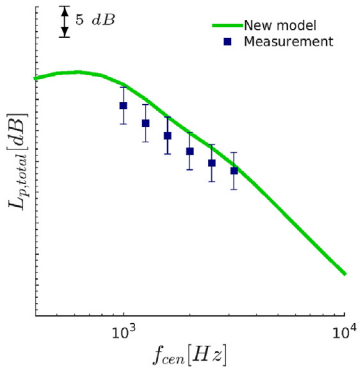

(a) Case TL231_45_00tSST corresponding to $U_\infty = 45\frac{m}{s}$ and $AoA = 0°$.

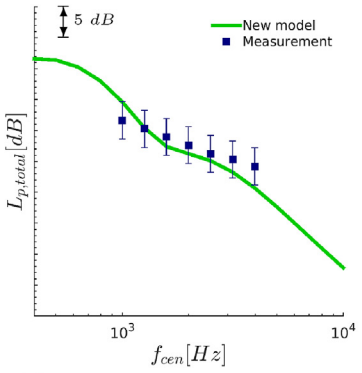

(b) Case TL231_45_35tSST corresponding to $U_\infty = 45\frac{m}{s}$ and $AoA = 3.5°$.

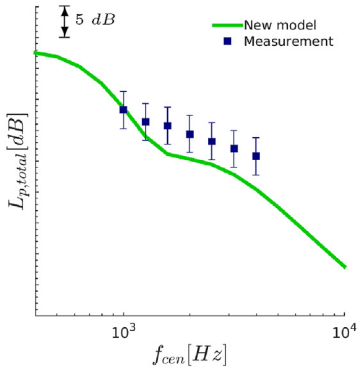

(c) Case TL231_45_45tSST corresponding to $U_\infty = 45\frac{m}{s}$ and $AoA = 4.5°$.

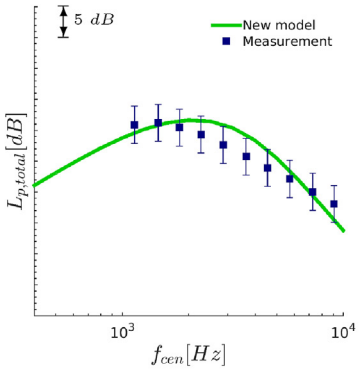

(d) Case NAC12_60_00tSST corresponding to $U_\infty = 60\frac{m}{s}$ and $AoA = 0.0°$.

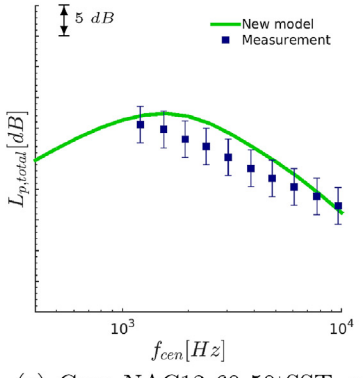

(e) Case NAC12_60_50tSST corresponding to $U_\infty = 60\frac{m}{s}$ and $AoA = 5°$.

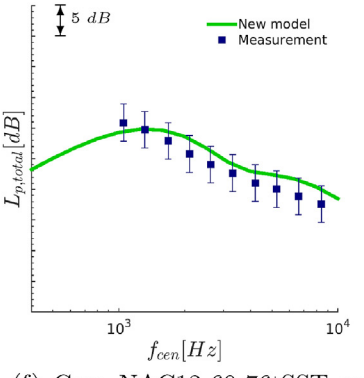

(f) Case NAC12_60_76tSST corresponding to $U_\infty = 60\frac{m}{s}$ and $AoA = 7.6°$.

Fig. 7. Comparison of experimental and predicted (new model) FF noise spectra.

cases, too. To keep this paper compact the comparison is shown by means of exemplary cases with the TL231 and NACA0012 airfoil only. However, during this research, cases for 5 other airfoils were investigated, which showed similar good results. Overall the new model shows an increased prediction accuracy for the cases evaluated in this section. It is not necessary to apply a semi-empirical modeling approach when taking into account the turbulence-turbulence interaction to predict the noise produced at high angles of attack. The enhanced prediction quality can also be seen when predicting the noise of a full rotor with the new model. Whilst this paper presents the theory of the new model, in Ref. [14] a study was conducted applying it to a multi-megawatt wind turbine and comparing the results with measurements.

To reduce TE noise both source terms, MTI and TTI, should be reduced. As discussed above, the TTI becomes relevant especially for boundary layers close to separation. For this reason an airfoil design should be chosen with a late laminar to turbulent transition and not too high pressure gradients in the pressure recovery region.

There are evidences that serrations also influence the TTI of a boundary layer [30]. However, most relevant for the noise reduction is a reduction of the overall turbulence level. This can be achieved by an adequate airfoil design but also by active methods such as boundary layer suction [10].

5. Conclusions

Trailing edge noise is considered to be one of the main noise sources of modern wind turbines. The widely used TNO model for trailing edge noise prediction is extended in the presented work to be applicable to high angles of attack and weakly separated flow. It is based on an equation for the wall pressure fluctuations on which an expression to account for far field effects is applied. The source equation for wall pressure fluctuations deduced from the continuity and the Navier-Stokes equations comprises two terms, the Mean-shear-Turbulence Interaction (MTI) and the Turbulence-Turbulence Interaction (TTI). In the commonly used TNO based prediction method the TTI is neglected. It was, however, identified to be one of the main parameters improving prediction quality for trailing edge noise at higher angles of attack and beginning boundary layer separation. Hence, a new equation for the wall pressure fluctuations is deduced, based on the whole source term equation for the wall pressure fluctuations, taking into account the TTI. The resulting additional terms are modeled based on turbulent parameters. In addition, a new modeling approach for the moving axis spectrum as well as an extension of the anisotropy formulation including the pressure gradient is presented, further improving the quality of the noise prediction.

The new model with all modifications is validated by comparing the prediction results to experiments conducted in different wind tunnels. It is applied to cases with different angles of attack, including cases with a slightly separated boundary layer. The test cases comprise two different airfoils and varying Reynolds numbers. The turbulent characteristics necessary for the models are extracted from RANS CFD simulations. It could be shown that the model is able to capture the increase in noise for higher boundary layer loadings and beginning trailing edge separation. It was found that the prediction quality for the suction side is better than for the accelerated flow close to the trailing edge on the pressure side. This difference is inherent to the TNO model and has been noted before.

Future research may explore the evaluation of LES simulations with higher angles of attack and, if possible, different airfoils to confirm the results presented here.

Acknowledgments

We thank the ENERCON GmbH Aurich for their continuous interest in our work and their financial support. Especially, we want to give our sincere thanks to Andree Altmikus and Christian Napierala for the time they spent in our fruitful discussions. Our gratitude also goes towards our colleague David Flad for providing us with the LES simulation results.

References

[1] W.K. Blake, Mechanics of Flow-Induced Sound and Vibration Volume I & II, Academic Press. Inc., Orlando, FL, 1986.
[2] R. Parchen, K. Looijmans, Progress Report DRAW, 1996.
[3] R. Parchen, T. N. O. I. O. A. Physics, Progress Report DRAW: a Prediction Scheme for Trailing Edge Noise Based on Detailed Boundary Layer Characteristics, 1998.
[4] T. Lutz, A. Herrig, W. Würz, M. Kamruzzaman, E. Krämer, Design and wind-tunnel verification of low-noise airfoils for wind turbines, AIAA J. 45 (4) (2007) 779–785, https://doi.org/10.2514/1.27658.
[5] M. Herr, Benchmarking of Trailing-Edge Noise Computations Outcome of the BANC-II Workshop, 2013, pp. 1–31, https://doi.org/10.2514/6.2013-2123.
[6] F. Bertagnolio, A. Fischer, W. Jun Zhu, Tuning of turbulent boundary layer anisotropy for improved surface pressure and trailing-edge noise modeling, J. Sound Vib. 333 (3) (2014) 991–1010, https://doi.org/10.1016/j.jsv.2013.10.008.
[7] M. Kamruzzaman, D. Bekiropoulos, A. Wolf, T. Lutz, E. Kramer, Rnoise: a RANS based airfoil trailing-edge noise prediction model, AIAA Conf. (2014) 1–22, https://doi.org/10.2514/6.2014-3305.
[8] M. Kamruzzaman, Study of Turbulence Anisotropy and its Impact on Flow Induced Noise Emission, Doctoral thesis, University of Stuttgart, 2012.
[9] A. Fischer, F. Bertagnolio, H.A. Madsen, Improvement of TNO type trailing edge noise models, in: ISROMAC, 2016.
[10] T. Lutz, B. Arnold, D. Bekiropoulos, J. Illg, E. Krämer, A. Wolf, R. Hann, M. Kamruzzaman, Prediction of flow-induced noise sources of wind turbines and application examples, Int. J. Aeroacustics 14 (5 & 6) (2015) 675–714.
[11] C.Y. Schuele, Trailing-Edge Noise Modeling and Validation for Separated Flow Conditions, 2013, pp. 1–13.
[12] F. Bertagnolio, H.A. Madsen, A. Fischer, C. Bak, A semi-empirical airfoil stall noise model based on surface pressure measurements, J. Sound Vib. 387 (2017) 127–162, https://doi.org/10.1016/j.jsv.2016.09.033.
[13] A. Suryadi, M. Herr, Wall pressure spectra on a DU96-W-180 profile from low to pre-stall angles of attack, in: 21st AIAA/CEAS Aeroacoustics Conference, 2015, pp. 1–18, https://doi.org/10.2514/6.2015-2688. http://arc.aiaa.org/doi/10.2514/6.2015-2688.
[14] C. Hornung, C. Scheit, C. Napierala, M. Arnold, D. Bekiropoulos, A. Altmikus, T. Lutz, Predicted and measured trailing-edge noise emission for a 2.3 MW wind turbine, in: Accepted for 7th International Conference on Wind Turbine Noise Rotterdam, 2017.
[15] D.M. Chase, Noise radiated from an edge in turbulent flow, AIAA J. 13 (8) (1975) 1041–1047, https://doi.org/10.2514/3.60502.
[16] T.F. Brooks, T.H. Hodgson, Trailing edge noise prediction from measured surface pressures, J. Sound Vib. 78 (1) (1981) 69–117, https://doi.org/10.1016/S0022-460X(81)80158-7.
[17] R.L. Panton, J.H. Linebarger, Wall pressure spectra for equilibrium boundary layer, J. Fluid Mech. 65 (1974) 261–287.
[18] J. Kim, On the structure of pressure fluctuations in simulated turbulent channel flow, J. Fluid Mech. 205 (1989) 421–451.
[19] Y.T. Lee, T.M. Farabee, W.K. Blake, Turbulence effects of wall-pressure fluctuations for reattached flow, Comput. Fluids 38 (5) (2009) 1033–1041, https://doi.org/10.1016/j.compfluid.2008.01.012.
[20] P.-A. Krogstad, P.E. Skare, Influence of a strong adverse pressure gradient on the turbulent structure in a boundary layer, Phys. Fluids 7 (8) (1995) 2014, https://doi.org/10.1063/1.868513. http://scitation.aip.org/content/aip/journal/pof2/7/8/10.1063/1.868513.
[21] Y. Rozenberg, G. Robert, S. Moreau, Wall-pressure spectral model including the adverse pressure gradient effects, AIAA J. 50 (10) (2012) 2168–2179, https://doi.org/10.2514/1.J051500.
[22] G.E. Elsinga, I. Marusic, The anisotropic structure of turbulence and its energy spectrum, Phys. Fluids 28 (2016), 011701, https://doi.org/10.1063/1.4939471.
[23] DLR, FLOWer Installation and User Manual. Version 2009.1, Tech. rep, 2006.
[24] A. Herrig, Validation and Application of a Hot-Wire Based Method for Trailing-Edge Noise Measurements on Airfoils, Ph.D. thesis, University of Stuttgart, 2010.
[25] M. Herr, R. Ewert, B. Faßmann, C. Rautmann, S. Martens, C.-h. Rohardt, A. Suryadi, Noise reduction technologies for wind turbines, in: A. Dillmann, G. Heller, E. Krämer, C. Wagner, S. Bansmer, R. Radespiel (Eds.), New Results in Numerical and Experimental Fluid Mechanics XI. Notes on Numerical Fluid Mechanics and Multidisciplinary Design, 136th Edition, Springer, Cham, 2018, pp. 611–621.
[26] A. Beck, T. Bolemann, David Flad, H. Frank, G.J. Gassner, F. Hindelang, C.-D. Munz, High-order discontinuous Galerkin spectral element methods for transitional and turbulent flow simulations, Int. J. Numer. Methods Fluid. 76 (8) (2014) 522–548.
[27] D. Flad, A.D. Beck, G. Gassner, C.-D. Munz, A discontinuous galerkin spectral element method for the direct numerical simulation of aeroacoustics, in: 20th AIAA/CEAS Aeroacoustics Conference, 2014, p. 2740.
[28] S.B. Pope, Turbulent Flows, Cambridge University Press, Cambridge, 2000, https://doi.org/10.1088/0957-0233/12/11/705 arXiv:arXiv:1011.1669v3.
[29] C. Bailly, G. Comte-Bellot, Turbulence, Springer International Publishing Switzerland, 2015.
[30] F. Avallone, S. Pröbsting, D. Ragni, Three-dimensional flow field over a trailing-edge serration and implications on broadband noise, Phys. Fluids 28 (11). https://doi.org/10.1063/1.4966633.